analytical chemistry

Technical Note

pubs.acs.org/ac

Free-Surface Microfluidics/Surface-Enhanced Raman Spectroscopy for Real-Time Trace Vapor Detection of Explosives

Brian D. Piorek,[†,‡] Seung Joon Lee,[†,‡] Martin Moskovits,[†] and Carl D. Meinhart*[,†,‡]

[†]Institute for Collaborative Biotechnologies, University of California, Santa Barbara, Santa Barbara, California 93106, United States

[‡]SpectraFluidics, Inc., 6950 Hollister Avenue, Santa Barbara, California 93117, United States

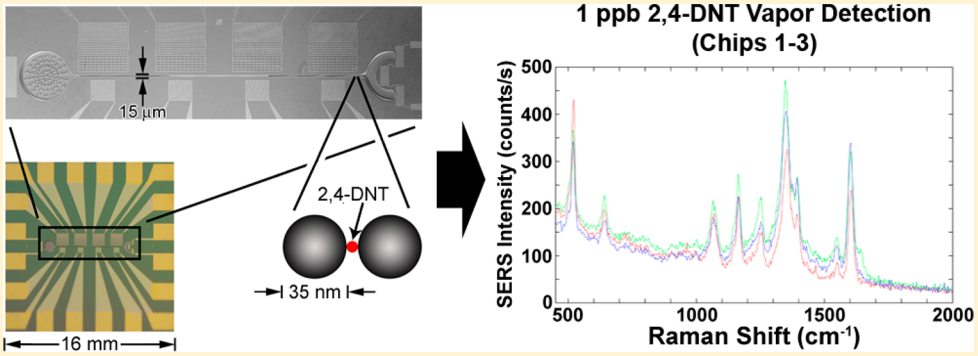

ABSTRACT: The dominant physical transport processes are analyzed in a free-surface microfluidic and surface-enhanced Raman spectroscopy (SERS) chemical detection system. The analysis describes the characteristic fluid dynamics and mass transport effects occurring in a microfluidic detection system whose analyte absorption and concentration capability is designed to operate on principles inspired by canine olfaction. The detection system provides continuous, real-time monitoring of particular vapor-phase analytes at concentrations of 1 ppb. The system is designed with a large free-surface-to-volume ratio microfluidic channel which allows for polar or hydrophilic airborne analytes to readily be partitioned from the surrounding gas phase into the aqueous phase for detection. The microfluidic stream can concentrate certain molecules by up to 6 orders of magnitude, and SERS can enhance the Raman signal by 9−10 orders of magnitude for molecules residing in the so-called SERS "hot spots", providing extremely high detection sensitivity. The resulting vibrational spectra are sufficiently specific to identify the detected analyte unambiguously. Detection performance was demonstrated using a nominal 1 ppb, 2,4-dinitrotoluene (2,4-DNT) vapor stream entrained within N_2 gas. Applications to homeland security arise from the system's high sensitivity and its ability to provide highly reproducible, continuous chemical detection monitoring with minimal sampling requirements.

The advancement of trace explosive vapor detection technology is a longstanding research goal with critical importance for homeland security and public safety. The performance standard for detection of trace explosive vapors is a sniffer dog (*Canis familiaris*). The canine's olfactory system has evolved to be a highly effective mechanism for absorbing and concentrating airborne chemical species present in low concentrations.[1] However, sniffer dogs are expensive to train, can tire easily, and can be unreliable, thus providing opportunities for novel analytical approaches. Current analytical methods for explosives detection can be broadly classified into either particle or vapor detection. Ion mobility spectroscopy (IMS) is a common particle detection method that is used in airport screening. For IMS detection of explosives, particulate matter is first collected by swabbing surfaces of interest. The swab is then heated to volatilize potentially collected analytes which may emanate vapors below the detection limit of IMS at ambient temperature. Once volatalized, the analyte is ionized and its mobility is measured in an electric field. Although this technique is the predominant analytical methodology in homeland security, its limited sensitivity requires the analyte to be physically collected in particulate form and heated before vapors emanating from explosive materials can be detected. Clearly it is advantageous to develop highly sensitive and specific sensor technologies which sample continuously at ambient vapor concentration levels, without the need to physically collect or heat the analyte beforehand.

Several developments in explosives detection technology have been reported within the past ten years. For instance, vapor detection technology based on the quenching of fluorescent polymers by certain airborne nitro compounds at levels as low as a few femtograms was developed by Bulovic et al.[2] Also, signal-to-noise ratio improvements in mass spectrometric devices have been reported by Denton.[3] Mass spectrometric devices have also been enhanced by using aerosol time-of-flight techniques[4] and desorption electrospray ionization.[5] Mass spectrometers, however, cannot easily be

Received: August 29, 2012
Accepted: October 16, 2012
Published: October 16, 2012

   dx.doi.org/10.1021/ac302497y | *Anal. Chem.* 2012, 84, 9700−9705

scaled down to the size of a hand-held device without significant performance degradation.

Trace detection of 2,4-dinitrotoluene (DNT) vapors is of widespread interest because it is formed by the substituent loss of a nitro group from the common high explosive trinitrotoluene (TNT). The vapor pressure of DNT (148 ppb at 20 °C) is 25 times higher than that of TNT (6 ppb at 20 °C).[6] As a result, the small quantities of DNT that emanate from TNT dominate the vapor headspace and serve as a natural tracer for TNT vapor detection.[7,8] Improved DNT vapor detection is therefore a rational goal for improved explosives detection in homeland security and public safety applications.

Surface-enhanced Raman spectroscopy (SERS), a form of vibrational spectroscopy which, as a result, provides molecule-specific data,[9−11] has been used to detect biomaterials and high explosives.[12,13] Detection of DNT by SERS has been reported by several groups: by the use of a KOH-roughened Au substrate[14] and on Au nanoparticle clusters with a thin NaOH liquid film.[15]

Microfluidic-based devices have gained significant popularity over the past 15 years. Advancements in microfabrication technology and improvements in fundamental understanding of micro- and nanoscale physics have facilitated lab-on-a-chip devices, in which miniscule quantities of material can be manipulated at the micro and nano scales. This reduction of scale provides a number of advantages, including (1) a significant reduction of analyte and reagent volumes and (2) the ability to conduct large numbers of chemical reactions simultaneously on a single monolithic chip.[16]

More recently, free-surface microfluidics was reported,[17,18] in which the microchannel is open to the surrounding atmosphere. Microfluidic flow is maintained by controlling the microchannel temperature at the ambient dew point. The flowing fluid is constrained within the channel by capillary forces. A SERS-active colloid is injected into the microchannel and SERS is used to detect static, high concentration 4-aminobenzenethiol vapor.[18] In the present study, we extend that initial work by developing a continuously sampling vapor detection system with unprecedented sensitivity and specificity. The detection system is optimized for security applications and is demonstrated by detecting vapor emanating for solid-phase 2,4-dinitrotoluene (2,4-DNT) at 1 ppb, which is less than 1% of the saturated 2,4-DNT headspace concentration at 20 °C.

Free-Surface Microfluidics/SERS Detection. Free-surface microfluidic (FSF) vapor detection is inspired by certain aspects of the canine olfactory system. The complex three-dimensional geometry of the nasal cavity provides a high interfacial area between the moving nasal cavity air and the static mucous layer.[1] This structure allows efficient transport of molecules from the air into the mucous layer, which confines and concentrates the airborne analyte molecules and thereby enhances their subsequent detection.[19,20]

The free-surface microfluidic detection system mimics many of the transport processes that occur in the canine nose. For example, the free-surface microchannel is 4−40 μm deep, which approximates the 5−30 μm deep mucous layer present in the nasal region of *C. familiaris*.[1] The essential principles of the system are illustrated in Figure 1. The green arrows indicate the incoming airstream containing analyte vapor. The airflow geometry is designed to provide a steady flow with a velocity of approximately U_∞ = 1 m/s. A boundary layer is developed on the microfluidic chip with a leading distance of L = 8 mm. The

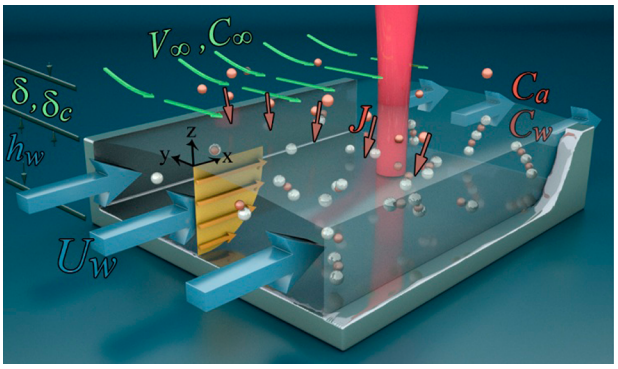

Figure 1. Cutaway illustration of material flows in the free-surface microfluidic channel. The aqueous microfluidic phase flows from left to right (blue arrows). The gas phase flows from back to front (green arrows). Analyte molecules (red spheres) diffuse from the gas phase into the liquid phase (red arrows). Nanoparticles (white spheres) suspended in the aqueous phase adsorb to suspended analyte molecules before interrogation by 658 nm laser light (red vertical beam) for detection by SERS.

boundary layer thickness can be estimated from Blasius' solution,

$$\frac{\delta}{L} = \frac{4.9}{\mathrm{Re}_L^{1/2}} \tag{1}$$

Assuming a kinematic viscosity for air $\nu_a = 1.51 \times 10^{-5}$ m^2/s, the Reynolds number can be estimated as $\mathrm{Re}_L \equiv (U_\infty L)/\nu$ = 530, and the boundary layer thickness is $\delta \approx 1.7$ mm.

The mass transfer coefficient for analyte transferring between the airstream and the microfluidic channel can be written as

$$k_c \equiv \frac{J}{c_\infty - c_a} = \frac{-D_a \partial c_a/\partial n|_{z=0}}{c_\infty - c_a} \tag{2}$$

where k_c is the aggregation constant of the colloid, J is the molar flux density, D_a is the analyte diffusivity in air, and c_a is the gas-phase analyte concentration. The derivative is taken with respect to the unit normal vector, n, and evaluated at the free-surface interface, z = 0. The difference in gas-phase concentration between the free stream and the free-surface interface is $c_\infty - c_a$. The local mass transfer coefficient can be calculated from the local Sherwood number, $\mathrm{Sh}_L \equiv (k_c L)/D_a$, where L is the location of the microfludic channel relative to the boundary layer leading edge. Using Blasius' solution for laminar boundary layers, the Sherwood number scales as

$$\mathrm{Sh}_L = 0.332 \mathrm{Re}_L^{1/2} \mathrm{Sc}^{1/3} \tag{3}$$

for Schmidt numbers $\mathrm{Sc} \equiv \nu_a/D_a \geq 0.6$.[21] Using the diffusivity of 2,4-DNT in air, $D_a = 2.03 \times 10^{-5}$ m^2/s, yielding Sc = 0.743. From eq 2, the Sherwood number is estimated to be Sh_L = 6.93, and the corresponding mass transfer coefficient through the air boundary layer is $k_c = 1.76 \times 10^{-2}$ m/s.

An ambient concentration of 1 ppb of 2,4-DNT at standard conditions (20 °C) corresponds to $c_\infty = 4.45 \times 10^{-8}$ mol/m^3. The ratio of the air and water concentrations at the free-surface interface can be estimated from the dimensionless form of Henry's law, $k_H \equiv c_a/c_w$, which for 2,4-DNT at standard conditions is $k_H = 3.8 \times 10^{-6}$.[22] The liquid region of the microchannel functions as a concentrator, effectively increasing the volumetric density of 2,4-DNT molecules which partition into the microchannel. Under equilibrium conditions, an

dx.doi.org/10.1021/ac302497y | *Anal. Chem.* 2012, 84, 9700−9705

ambient 2,4-DNT concentration of 1 ppb ($c_\infty = 4.45 \times 10^{-8}$ mol/m^3) produces a maximum aqueous concentration of $c_w = c_a/k_H = 11.7$ μM, which is sufficient for the analyte to adsorb onto nanoparticles and become detectable using SERS. Accounting for Henry's law, molar flux density can be written as

$$J = k_c[c_\infty - (k_H c_w)] \tag{4}$$

Consider a shallow, $h_w = 4 \times 10^{-6}$ m microchannel, in which the analyte can readily diffuse throughout the depth of the channel. The timescale for vertical diffusion can be estimated as $\tau_{diff} \sim h_w^2/6D_w = 1/6 \times (4 \times 10^{-6}\ \text{m})^2/(7.06 \times 10^{-10}\ \text{m}^2/\text{s}) = 3.8$ ms, where D_w is the diffusivity of 2,4-DNT in water. Using eq 4, the depth-averaged analyte concentration $\bar{c}_w$ satisfies the steady depth-averaged convective scalar equation with an average velocity of the aqueous phase, $\bar{u}_w$

$$\bar{u}_w \frac{d\bar{c}_w}{dx} = \frac{k_c}{h_w}[\bar{c}_\infty - k_H \bar{c}_w] \tag{5}$$

The limited microfluidic channel depth (4 μm) is designed to produce a high surface-to-volume ratio, causing the parameter k_c/h_w to be large. The large surface area allows analyte molecules to readily partition into the liquid, while the relatively small volume limits analyte dilution. The absorption time to reach a nominal 2,4-DNT concentration of $\bar{c}_w = 1$ μM is approximately $\tau_f = (h_w\bar{c}_w)/(k_c\bar{c}_\infty) \approx 5$s.

The free-surface microfluidic flow (Figure 1, blue arrows) is controlled by capillary forces by use of a transpirational-type pump,[23] and has a nominal velocity of $\bar{u}_w \approx 500 \times 10^{-6}$ m/s. Therefore, the microfluidic flow travels a distance of approximately 2.5 mm downstream in order to reach a 2,4-DNT concentration of $\bar{c}_w = 1$ μM.

Multiscale Control of Nanoparticle Kinetics. Nanoparticle control within the system is achieved by hierarchical design, whereby each design element allows control of the next smaller element. This hierarchy of the length scales is illustrated in Figure 2, where the microfluidic chip has a length scale on the order of 10 mm which controls the fluid motion with depths on the order of 4–40 μm. In turn, the microfluidic flow controls the aggregation of the approximately 35 nm diameter nanoparticles.

It is through this use of the successive length scales (from millimeters to micrometers to tens of nanometers) that one can precisely control the motion and aggregation of the nanoparticles in a practical manner.

The nanoparticle-based, SERS-active colloid flows continuously through the microfluidic channel, thereby providing a continuously refreshing SERS substrate. This microfluidic substrate refreshment provides for continuous, real-time, long-term (>1 h) gaseous-headspace chemical detection monitoring since the SERS-active region is continuously refreshed during operation. We term this design a "dynamic SERS substrate" since the SERS-active material is moving in order to provide a continuous replenishment mechanism. The most intense SERS signals are now known to originate from molecules resident in so-called "hot spots", which are often interstitial sites (e.g., gaps and clefts) between nanoparticle aggregates.

Within the microchannel flow, absorbed 2,4-DNT molecules adsorb onto the Ag nanoparticles. These moieties in turn self-assemble with increasing time (i.e., streamwise distance from the nanoparticle inlet.) The resulting aggregation kinetics can

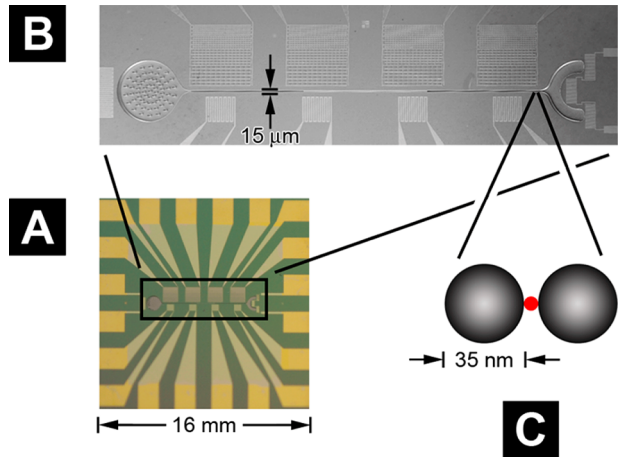

Figure 2. Implementation of the free-surface microfluidics/SERS detection system. Each subfigure shows the hierarchy of the length scales used, ranging from tens of millimeters to tens of nanometers. (A) Photograph of the Si-based microfluidic chip which contains the free-surface channel, on-chip temperature sensors, and on-chip humidity sensors. An electronic readout is established using the Au connection pads along the chip edge. (B) SEM image showing the detail of the free-surface microfluidic channel and sensors. The channel is 4–40 μm deep and approximately 6 mm long. The microfluidic flow moves from left to right. (C) Cartoon of two approximately 35 nm diameter Ag nanoparticles encompassing an analyte molecule, forming a so-called SERS "hot spot".

be described by the conserved scalar equation for depth-averaged nanoparticle-aggregate concentrations

$$\bar{u}_w \frac{\partial \bar{c}_i}{\partial x} = \nabla\cdot(D_i \nabla \bar{c}_i) + R_i \tag{6}$$

where $\bar{c}_i$ is the concentration of nanoparticle monomers, dimers, trimers, tetramers, etc. The reaction terms are approximated by second-order reaction kinetics and a simplified single affinity constant, k.

$$\begin{aligned} R_1 &= -2k(\bar{c}_1\bar{c}_1) - k(\bar{c}_2\bar{c}_1) - k(\bar{c}_3\bar{c}_1) \\ R_2 &= k(\bar{c}_1\bar{c}_1) - k(\bar{c}_2\bar{c}_1) - 2k(\bar{c}_2\bar{c}_2) \\ R_3 &= k(\bar{c}_2\bar{c}_1) - k(\bar{c}_3\bar{c}_1) \end{aligned} \tag{7}$$

Self-assembly is induced by the adsorption of analyte, $\bar{c}_w$, onto nanoparticle surfaces. This adsorption displaces the homogeneously distributed citrate ions resident initially on nanoparticle surfaces in the aqueous suspension,[24] thereby reducing the repulsive Coulombic barrier to aggregation. The dimerization rate constant as a function of analyte concentration is assumed to be

$$k = k_o\, e^{-V_o/(K_b T(1+\beta\bar{c}_w)^{12/5})} \tag{8}$$

where the constants k_o, V_o, and β can be determined empirically. Entrained 2,4-DNT molecules are well-suited to drive the nanoparticle self-assembly process since the nitro groups on the 2,4-DNT bond readily to the silver nanoparticle surfaces.[25,26]

Plasmon resonances induced by optical laser stimulation cause strong electromagnetic field enhancement between adjacent dimerized nanoparticle surfaces, forming SERS "hot spots" in these regions. The resulting SERS electromagnetic field enhancement can be from 10^9 to 10^{10}, thereby providing

dx.doi.org/10.1021/ac302497y | Anal. Chem. 2012, 84, 9700–9705

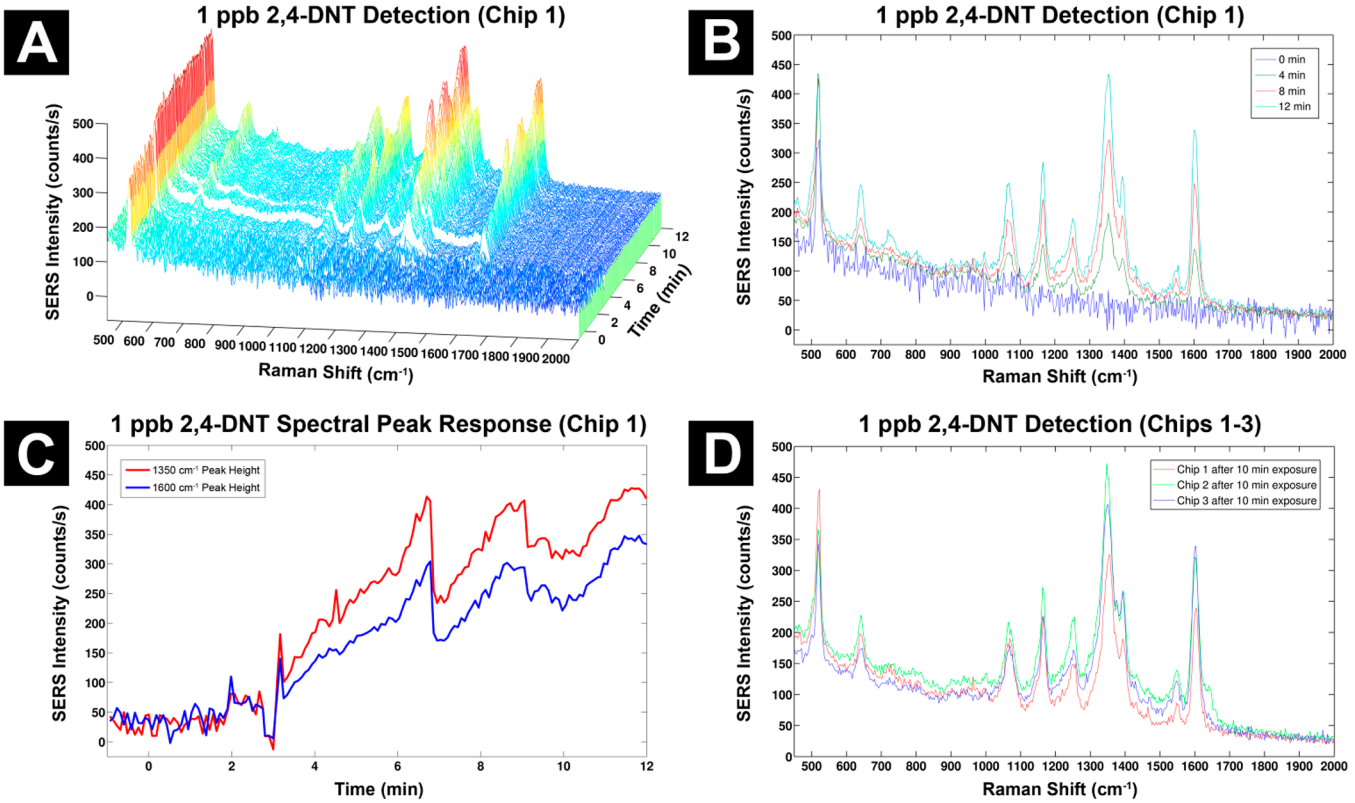

Figure 3. Raw, unprocessed spectral data resulting from the detection of 2,4-DNT (1 ppb 2,4-DNT, 40% relative humidity). (A) 2,4-DNT SERS spectra obtained by the free-surface microfluidic system during test 1. (B) Overlay of selected raw spectra from test 1. (C) Temporal response at 1350 cm^{-1} (NO_2 symmetric stretch response) and 1600 cm^{-1} (NO_2 asymmetric stretch + benzene ring in-plane stretch response) during test 1. The 2,4-DNT analyte flow was activated at time $t = 0$ s. (D) Overlay of raw spectra obtained after 10 min from three separate experiments. We note that the intensity of chip 1 is approximately 25% lower than the intensity of chip 2 after performing a simple background subtraction from each spectrum.

intense Raman spectra from low numbers of molecules adsorbed to the nanoparticles.[27]

EXPERIMENTAL SECTION

The microfluidic device shown in Figure 2 was microfabricated in ⟨100⟩ Si by typical MEMS microfabrication procedures. The microchannel was designed to be 15 μm wide and 6 mm long. The microchannel was divided into three successive regions, each being 2 mm in length. The first and third regions were 40 μm deep, while the middle region was relatively shallow at only 4 μm deep.

The free-surface microfluidic channel was cooled to the dew point by feedback control (National Instruments, model no. DAQPad-6259) using a thermoelectric cooler (Tellurex, model no. CZ1-1.0-127-1.27) located underneath the microchip. The microchip temperature was maintained near the dew point by monitoring microchip surface wetness with an electrical sensor microfabricated on the microchip surface. The sensor was an interdigitated electrode, whose impedance indicated surface wetness. The resulting measured surface wetness value was maintained at a constant, partially wet state by manipulation of the thermoelectric cooler temperature set point.

The liquid flow within the microchannel was driven by Joule heating from a microfabricated electrical heater element which was located at the distal end of the microchannel. The heater formed a transpirational pump,[23] which drove the microchannel flow by evaporation-driven water loss at the distal end of the 6 mm long microchannel. Microchannel flow velocity was confirmed to scale linearly with the evaporator heater power over the range of 0−500 μm/sec by micro particle image velocimetry.[28]

To produce SERS "hot spots" within the free-surface microfluidic flow, a 1 nM solution of 35 nm diameter nanoparticles[29] was flowed through the FSF microchannel at ∼500 μm/s. A confocal spectrometer with 658 nm, 35 mW excitation source was used to interrogate the microfluidic channel (model no. R660, SpectraFluidics, Inc.)

2,4-DNT vapor was generated by passing N_2 gas (Airgas LLC USA, model no. BIP300, 99.9999% pure) through a curved glass tube (arc length: 6", ID: 5 mm, total distance between analyte and microfluidic chip: 8") filled with 500 mg of 2,4-DNT powder (Sigma-Aldrich, 99.2% pure). Equilibrium was assumed between the solid and gaseous 2,4-DNT phases, whereby the resulting concentration is calculated by Antoine's equation and Raoult's law. The resulting analyte stream is diluted with pure N_2 gas[30] and mixed with humidified N_2 to produce nominally 1 ppb 2,4-DNT vapor at 40% relative humidity. Sample delivery system gas flows were controlled with computer-controlled mass flow controllers (Omega Engineering, Inc., model no. FMA-5514). The total gas delivery rate was 0.8 L/min. From this stream, a 0.4 L/min gaseous analyte stream was injected into the headspace above the microfluidic chip using a small metering pump.

Great care was exercised to avoid contamination of the microfluidic system and analyte delivery system before and during the tests. Precautions included the final cleaning of the sample delivery glassware with a UVO cleaner (model no. 42,

dx.doi.org/10.1021/ac302497y | Anal. Chem. 2012, 84, 9700−9705

Jelight Company, Irvine CA) for 10 min immediately before use and the use of fresh DNT samples for each test.

RESULTS AND DISCUSSION

Background spectral data were collected continuously for 6.7 min before the 2,4-DNT analyte was introduced into the gas stream for detection. No significant SERS peaks were observed during this time, indicating that neither the N_2 carrier gas nor the working colloidal fluid yield a spectral response when no analyte is present. The first 5.7 min of background data are therefore not presented because the data were unremarkable. The experimental procedures for test 1, test 2, and test 3 were similar.

The spectral results are shown in Figure 3. Figure 3A shows the SERS spectra for the 2,4-DNT measurements as a function of wavenumber (cm^{-1}), and experiment time (min). The 1 ppb 2,4-DNT analyte was introduced into the gas stream at time t = 0 s. Distinct peaks within the SERS spectra first appear at approximately t = 2 min. An intense 2,4-DNT spectrum is present at t = 3 min.

Figure 3B shows selected raw spectra from test 1, for times t = 0, 4, 8, and 12 min. No processing was carried out on the spectra shown, so as to illustrate the actual signal-to-noise ratio of the detector. At t = 2 min, the first spectral response was observed.

Characteristic NO_2 vibrations appear at ~1350 cm^{-1} (NO_2 symmetric stretch) and ~1560 cm^{-1} (NO_2 asymmetric stretch + ring in-plane stretch). Other bands are attributed to vibrations of the benzene ring: 625 cm^{-1} (CH_3 in-plane bend + CN rock), 1040 cm^{-1} (CH_3 and CH wag), 1140 cm^{-1} (CN stretch + ring in-plane stretch + CH_3 rock), 1230 cm^{-1} (ring breathing + CH in-plane bend), and 1600 cm^{-1} (NO_2 asymmetric stretch + ring in-plane stretch).[31,32] The band at 520 cm^{-1} results from the bulk Si substrate of the microfluidic channel.

The two most significant spectral peaks observed in Figure 3B occur at 1350 cm^{-1} and 1600 cm^{-1}. The intensity of these two peaks is plotted as a function of time in Figure 3C. The intensities of these two peaks fluctuate in response to the stochastic variation of the observed nanoparticle aggregates. These peaks vary together and are a good summary indication of the detected signal, starting at t = 2 min and reaching maximum intensity at t = 6.5 min.

System reproducibility is demonstrated by comparing spectra from three separate experiments: test 1, test 2, and test 3 at time t = 10 min. The raw spectrum collected at t = 10 min during each of the three experiments is shown in Figure 3D. The results indicate a similar spectral response over all three tests.

Since the SERS detection mechanism is not sensitive to water, microchannel fluid does not contribute to the spectral response as shown in Figure 3. The signal-to-noise ratio of all three chips exceeds 20:1 after a 10 min exposure to 2,4-DNT (Figure 3D).

The DNT spectra obtained from tests 1−3 (Figure 3D) are in good concordance. The significant peaks are in agreement with published literature values, providing unambiguous identification of 2,4-DNT. Detection response time is approximately 2 min.

The operation of the free-surface microchannel detector requires the chip to be maintained at the dew point of the gas-phase analyte stream, which was controlled by feedback. While operating, the FSF−SERS system is a "dynamic SERS substrate" utilizing a continually refreshing colloid, which can significantly decrease photo/thermal degradation of entrained 2,4-DNT or other analytes.

CONCLUSIONS

A novel free-surface microfluidic/SERS system is described and analyzed for detecting trace levels of vapor-phase molecules within a continuously flowing gas stream. The microfluidic-based, SERS-active substrate produced by the system is continuously refreshed. Gaseous analyte molecules absorb into the free-surface microfluidic flow and adsorb onto the nanoparticles, thereby inducing aggregation of the colloid. The resulting system provides a new paradigm for SERS detection of explosives vapors, which is compatible with ambient humidity levels existing at typical screening applications such as airports and public venues.

The microfluidic channel is designed to be very shallow, ranging from 4−40 μm so as to provide a large surface-to-volume ratio, increasing the subsequent concentration of the resulting aqueous analyte and allowing for trace level chemical detection. The mass transfer coefficient of an airborne analyte to the free-surface microfluidic interface is limited by the Sherwood number associated with the laminar airstream boundary layer. Once the analyte is transported to the free liquid surface, polar or hydrophilic molecules partition through the free surface with greater propensity than nonpolar or hydrophobic molecules. For example, the ratio of Henry's constants for toluene and 2,4-DNT indicates approximately a 5 orders of magnitude preference for 2,4-DNT as compared to toluene.

The high chemical detection sensitivity of the microfluidic/SERS system is partially due to the concentrating effect resulting from the partitioning of polar or hydrophilic molecules. For 2,4-DNT, this concentration effect is approximately 6 orders of magnitude, according to the published Henry's Law constants. When the analyte reaches a sufficient aqueous concentration within the microfluidic flow, aggregation of the SERS-active colloid occurs which produces SERS "hot spots". These "hot spots" amplify the Raman signal intensity by factors as large as 10^9−10^{10}, further contributing to the high chemical detection sensitivity of the system.

System efficacy was demonstrated by routine detection of the vapor phase 2,4-DNT entrained in nitrogen at levels of 1 ppb, which is less than 1% of the saturated headspace concentration of neat 2,4-DNT. The FSF−SERS system responded within 2 min of exposure, reaching a signal-to-noise ratio that exceeded 20:1 within 10 min after initial analyte exposure.

AUTHOR INFORMATION

Corresponding Author

*E-mail: meinhart@engineering.ucsb.edu

Notes

The authors declare no competing financial interest.

ACKNOWLEDGMENTS

The authors thank Dr. Augustus W. Fountain, Dr. Steven Christesen, Dr. Jason Guicheteau, and Mr. Darren Emge from Edgewood Chemical Biological Center, Aberdeen Proving Ground, for their many helpful discussions regarding the detection of 2,4-DNT. The authors also thank Mr. Nicholas Judy and Mr. Sean Demura of UCSB for fabricating the microfluidic chips. The authors also thank Mr. John Day and

Mr. Brian Dunne of SpectraFluidics for providing technical support. This work was supported in part by SpectraFludics, Inc. and the Institute for Collaborative Biotechnologies through contract no. W911NF-09-D-0001 from the U.S. Army Research Office, and contract no. W31P4Q-09-1-001 from DARPA. The content of the information herein does not necessarily reflect the position or policy of the Government and no official endorsement should be inferred.

REFERENCES

(1) Craven, B. A.; et al. *The Anatomical Record* **2007**, *290*, 1325−1340.
(2) Rose, A.; Zhu, Z.; Madigan, C. F.; Swager, T. M.; Bulovic, V. *Nature* **2005**, *434*, 876−879.
(3) Denton, D. B. *Advanced Instrumental Technologies and their Impact on Homeland Security and on Forensic Science*, The 229th ACS National Meeting, American Chemical Society: San Diego, CA, Mar. 13−17, 2005; http://oasys2.confex.com/acs/229nm/techprogram/P838120.HTM, accessed October 2012.
(4) Yongxuan, S. *Aerosol Sci. Technol.* **2006**, *40*, 3912−3921.
(5) Takats, Z.; Wiseman, J. M.; Gologan, B.; Cooks, R. G. *Science* **2004**, *15* (306), 471−473.
(6) Pella, P. A. *Anal. Chem.* **1976**, *48*, 1632.
(7) Fountain, A. W., III; Oyler, J. M.; Ostazeski, S. A. *Proc. SPIE* **2008**, *6954*, 695402.
(8) Edge, C. C.; Gibb, J.; Wasserzug, L. S. *Proc. SPIE* **1998**, *3392*, 502.
(9) Moskovits, M. *Rev. Mod. Phys.* **1985**, *57* (3), 783−828.
(10) Fleischman, M.; Hendra, P. J.; McQuillan, A. J. *Chem. Phys. Lett.* **1985**, *26*, 123.
(11) Jeanmaire, D. L.; Van Duyne, R. P. *J. Electroanal. Chem.* **1977**, *84*, 1.
(12) Guicheteau, J.; et al. *Appl. Spectrosc.* **2008**, *62*, 3.
(13) Steinfeld, J. I.; Wormhoudt, J. *Annu. Rev. Phys. Chem.* **1998**, *49*, 203−32.
(14) Sylvia, J. M.; Janni, J. A.; Klein, J. D.; Spencer, K. M. *Anal. Chem.* **2000**, *72*, 5834−5840.
(15) Wang, J.; Yang, L.; Boriskina, S.; Yan, B.; Reinhard, B. M. *Anal. Chem.* **2011**, *83* (6), 2243−2249.
(16) Thorsen, T.; Maerkl, S. J.; Quake, S. R. *Science* **2002**, *298* (593), 580−585.
(17) Piorek, B. D.; Mechler, A.; Lal, R.; Freudenthal, P.; Meinhart, C. D.; Banerjee, S. *Appl. Phys. Lett.* **2006**, *89*, 153123−153125.
(18) Piorek, B. D.; Lee, S. J.; Santiago, J. G.; Moskovits, M.; Banerjee, S.; Meinhart, C. D. *Proc. Nat. Acad. Sci. U.S.A.* **2007**, *104*, 18898−18901.
(19) Stitzel, S. E.; Stein, D. R.; Walt, D. R. *J. Am. Chem. Soc.* **2003**, *125*, 3684−3685.
(20) Correa, J. E. *The Dog's Sense of Smell*. http://www.aces.edu/pubs/docs/U/UNP-0066 (accessed 2005).
(21) Incropera, F. P.; DeWitt, D. P. *Fundamentals of Heat and Mass Transfer*, 3rd Ed.; John Wiley & Sons: New York, 2005.
(22) Part 5: Chemical-Specific Parameters. http://www.epa.gov/superfund/health/conmedia/soil/pdfs/part_5.pdf, accessed February 2012.
(23) Effenhauser, C. S.; Harttig, H.; Krämer, P. *Biomed. Microdevices* **2002**, *4* (1), 27−32.
(24) Faulds, K.; et al. *Anal. Chem.* **2004**, *76* (592), 592−598.
(25) Moskovits, M.; Vlčková, B. *J. Phys. Chem. B* **2005**, *109*, 14755−14758.
(26) Vlčková, B.; Gu, X. J.; Tsai, D. P.; Moskovits, M. *J. Phys. Chem.* **1996**, *100*, 3169−3174.
(27) Xu, H.; Aizpurua, J.; Käll, M.; Apell, P. *Phys. Rev. E.* **2000**, *62*, 4318−4324.
(28) Meinhart, C. D.; Wereley, S. T.; Santiago, J. G. *Exp. Fluids* **1999**, *27*, 414−419.
(29) Lee, P. C.; Meisel, D. *J. Phys. Chem.* **1982**, *86* (17), 3391−3395.
(30) Bonnot, K.; et al. *Anal. Chem.* **2010**, *82*, 3389−3393.
(31) Ramos, C. M.; et al. *J. Mol. Struct.: THEOCHEM* **2006**, *769*, 69−76.
(32) Clarkson, J.; et al. *J. Mol. Struct.* **2003**, *648* (3), 203−214.